

RSC Advances



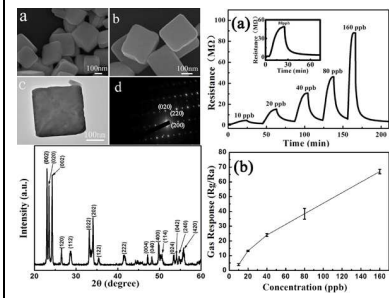
This is an *Accepted Manuscript*, which has been through the Royal Society of Chemistry peer review process and has been accepted for publication.

Accepted Manuscripts are published online shortly after acceptance, before technical editing, formatting and proof reading. Using this free service, authors can make their results available to the community, in citable form, before we publish the edited article. This *Accepted Manuscript* will be replaced by the edited, formatted and paginated article as soon as this is available.

You can find more information about *Accepted Manuscripts* in the [Information for Authors](#).

Please note that technical editing may introduce minor changes to the text and/or graphics, which may alter content. The journal's standard [Terms & Conditions](#) and the [Ethical guidelines](#) still apply. In no event shall the Royal Society of Chemistry be held responsible for any errors or omissions in this *Accepted Manuscript* or any consequences arising from the use of any information it contains.

A simple solvothermal method was used to the synthesis of WO_3 , which exhibited a good response to NO_2



Cite this: DOI: 10.1039/c0xx00000x

www.rsc.org/xxxxxx

ARTICLE TYPE

One-pot synthesis of cuboid WO₃ crystal and its gas sensing propertiesChong Wang^a, Xin Li^a, Biao Wang^b, Jian Ma^a, Yang Cao^a, Yanfeng Sun^{a*}, Geyu Lu^{a*}*Received (in XXX, XXX) Xth XXXXXXXXX 20XX, Accepted Xth XXXXXXXXX 20XX*

In this work, a simple solvothermal method was used to the synthesis of cuboid WO₃ crystal without any surface active agent. The calcined WO₃ was characterized using field emission scanning electron microscopy (FESEM), X-ray powder diffraction (XRD) and transmission electron microscopy (TEM). These results indicate that the sample is composed of cuboid nanobulks. Gas sensing property of the sensor based on the cuboid WO₃ was also investigated. It is found that the sensor has a high response to low concentration NO₂ at low operation temperature. So the cuboid nanobulks might have a potential application to fabricate highly sensitive and low power consumption NO₂ gas sensor.

Keywords: solvothermal; tungsten oxide; nanostructure; NO₂; sensor.

1. Introduction

With the increasing attention on atmospheric pollution, how to fulfill the detection of harmful gases with low concentration becomes an important issue. So, a lot of effort has been devoted to the exploration of new material with enhanced gas sensing performance in recent years. The existing gas sensor materials include semiconducting metal oxides¹⁻², silicon³⁻⁴, organic⁵⁻⁶ and fiber optic chemical materials⁷⁻⁸. Among them, semiconducting metal oxides have gained much more focus due to their superior properties. Up to now, a variety of semiconductor nanomaterials have been successfully synthesized, such as ZnO⁹⁻¹⁰, SnO₂¹¹⁻¹², CuO¹³⁻¹⁴, Fe₂O₃¹⁵⁻¹⁶ and In₂O₃¹⁷⁻¹⁸. As is well known, NO₂ is a highly harmful gas among the toxic gases which can cause acid rain and photochemical smog, and further affect people's health, even the life. And WO₃ is found to show high response to NO₂ with high selectivity¹⁹⁻²⁰. However, it is still a challenge to achieve high response to ppb level of NO₂.

In order to improve the performance of the sensors based on WO₃, various structures with different morphologies have been investigated: nanoplates²¹, nanorods²², nanospheres²³, nanoflowers²⁴ and other hierarchically complex architectures. At the same time, different physical and chemical synthetic methods have also been explored to obtain WO₃ crystals²⁵⁻²⁸. Among all these methods, the solvothermal method is concerned as a simple and practicable operation to synthesize high yield crystals with good monodispersity. Moreover, the low-cost synthesis is also the key point of the researchers' pursuit all the time. Consequently, it is strongly desirable to develop a simple, effective, and economical approach for the synthesis of WO₃ with excellent sensing performance to NO₂.

Herein, we report a facile method for the preparation of WO₃ crystal by a simple process. And the sensing performance based on the calcined WO₃ nanocrystal is also investigated here.

It is found that the sensor showed a high response to ppb level of NO₂ at 100°C.

2. Experimental*2.1. Synthesis and characterization of WO₃ nanobulks*

All the reagents (analytical-grade purity) were used without any further purification. In a typical synthesis, 10 mL glycerol and 25 mL distilled water were mixed together under the condition of stirring. One hour later, 0.66g sodium tungstate was added to the solution to form a homogeneous solution. And then, 2.5 mL 12 M HCl was dropped to the sodium tungstate solution and the yellow precipitates were formed. Five minutes later, the above solution was transferred into a Teflon-lined stainless steel autoclave, sealed tightly, and maintained at 180°C for 12 h. After the autoclave was cooled to room temperature naturally, the precipitates were washed with deionized water and absolute ethanol for several times using centrifuge, and then dried at 80°C for 24 h. The precipitates were calcined at 500°C for 2 h with a heating rate of 2°C/min. The calcined products were then collected for further analysis.

X-ray power diffraction (XRD) analysis was conducted on a Rigaku D/max-2500 X-ray diffractometer with Cu K α 1 radiation ($\lambda = 1.54056 \text{ \AA}$) in the range of 20-60°. The morphology was examined by field-emission scanning electron microscopy (FESEM, JEOL JSM-7500F, operated at an acceleration voltage of 15 kV). Transmission electron microscopy (TEM), selected-area electron diffraction (SAED) were obtained on a JEOL JEM-2100 microscope operated at 200 kV.

2.2. Fabrication and measurement of sensor

The calcined powders were mixed with deionized water to form a paste which was then coated onto an alumina tube (4 mm in length, 1.2 mm in external diameter and 0.8 mm in internal diameter) using a small brush slowly and lightly. The tube was installed with a pair of gold electrodes, and each electrode was connected with two Pt wires. After brushing, a thick film was formed. After drying at room temperature, the sensing device was then sintered at 300°C for 2h in air. Finally, a Ni-Cr alloy coil was inserted into the alumina tube as a heater in order to control the operating temperature of the sensor. A schematic structure of the as-fabricated sensor was shown in Fig. 1a.

The gas sensing property of the sensor was measured by a static process, and the schematic diagram is given in Fig. 2b. The resistance in the chamber (the volume is 50L) filled with air is Ra, and then a certain amount of target gas is injected into this closed chamber. When the resistance reached Rg, the gas is discharged under the help of air blower and fan. The data is collected by digital precision multimeter every second. $S=Rg/Ra$ is defined as the response of the sensor for oxidizing gas and Ra/Rg for reducing gas, here, Ra and Rg is the resistance of the sensor in the air and target gas.

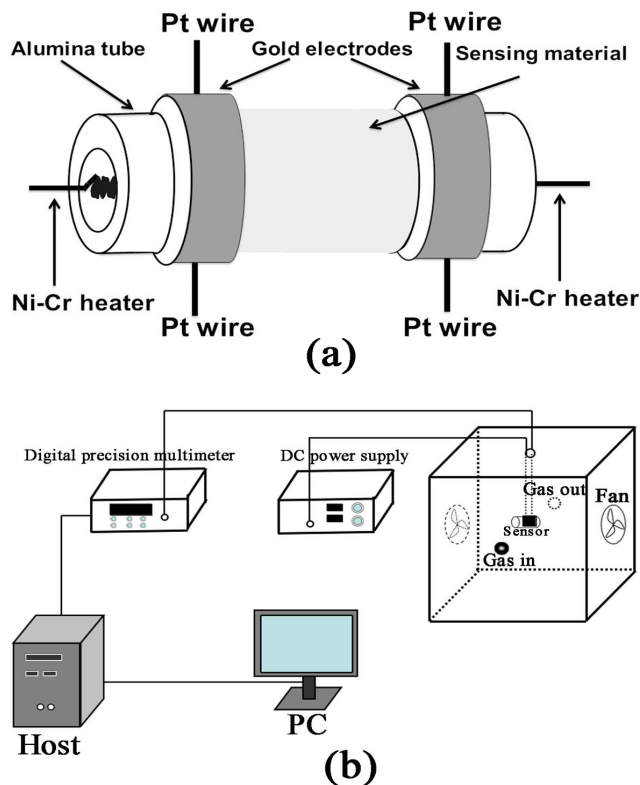


Fig. 1. (a) Schematic structure of the gas sensor. (b) The testing schematic diagram

3. Results and discussion

3.1. Structural and morphological characteristics of the calcined WO_3

The X-ray diffraction (XRD) patterns of the calcined products are shown in Fig. 2. It can be seen from Fig. 2 that all of the diffraction peaks can be well indexed to the standard WO_3 (JCPDS file No.83-950). No other diffraction peaks from any impurities are observed, indicating the high purity of the product. And the XRD patterns (not shown here) of the sample without calcination are almost the same as the calcined products.

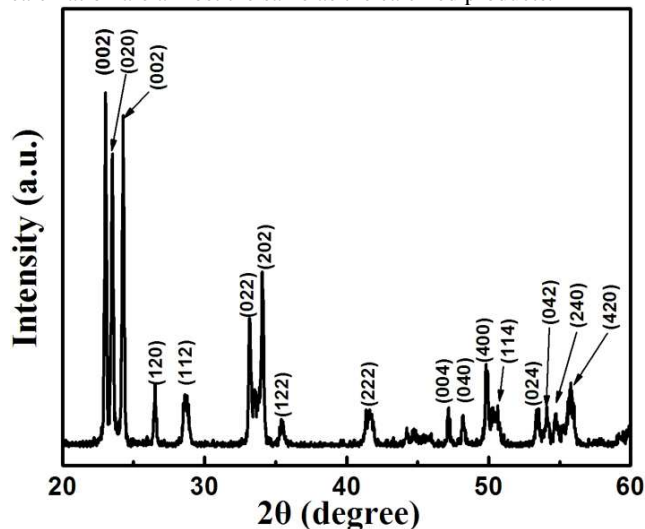


Fig. 2. X-ray diffraction patterns of the calcined product.

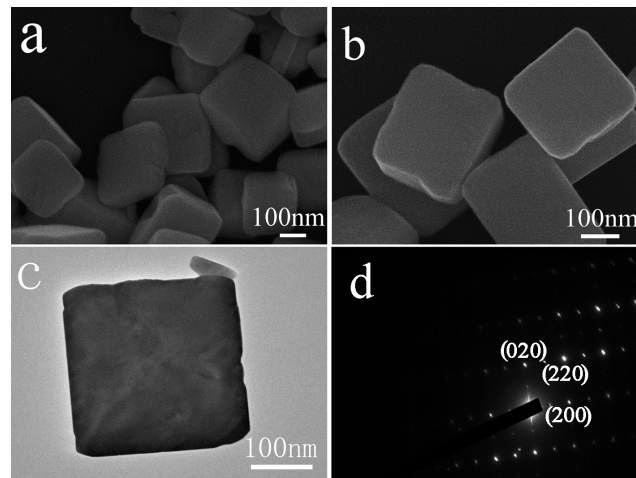


Fig. 3. (a) and (b) Typical SEM images of the calcined product (c) TEM image of the WO_3 cuboid nanobulks (d) The corresponding SAED pattern.

The morphology of the calcined product was investigated by field emission scanning electron microscopy (FESEM). The typical SEM images are shown in Fig. 3a and Fig. 3b. As can be seen from Fig. 3a and Fig. 3b, the products are mostly composed of cuboid three-dimensional nanobulks. The TEM image is shown in Fig. 3c, an individual typical cuboid three-dimensional nanobulks is also observed, which is agreed with the SEM results. The selected area electron diffraction pattern (SAED) was also performed on the calcined products, as shown in Fig. 3d, which confirmed that the nanobulks are single crystalline of monoclinic WO_3 .

3.2. Gas-Sensing Properties for NO_2

The sensing properties of the sensor based on the as-prepared WO_3 samples were investigated. In order to determine the optimum operating temperature, the response of the sensor to 80 ppb NO_2 was measured at different temperatures. As shown in Fig. 4, the response of the sensor increases from 75°C to 100°C. When the temperature further increases above 100°C, the response begins to decrease gradually. This phenomenon could be explained as follows: at low temperature (between 75°C and 100°C), the increase of the response can be attributed to the increase of the surface reaction ($\text{NO}_{2(\text{g})} + \text{e}^- \rightarrow \text{NO}_{2(\text{ads})}^-$). Such adsorption can capture the electrons from WO_3 and resulting in the increasing of the electrical resistance. However, when the temperature is higher (between 100°C and 200°C), the chemi-adsorbed oxygen becomes larger and plays a significant role ($\text{O}_{(\text{ads})}^{2-} + \text{NO}_2 \rightarrow \text{NO}_{2(\text{ads})}^- + \text{e}^-$), this kind of reaction goes against the adsorption of NO_2 . On the other hand, the rate of adsorption is lower compared to desorption at the higher temperature, which might be another reason for the decrease of the sensor's response³⁵⁻³⁷. Accordingly, at the temperature of the maximum response, the optimum balance between adsorption and desorption has been established for the NO_2 molecules. Therefore, the optimal working temperature of 100°C is chosen to further exam the characteristics of the gas sensor.

The response transient curve of the sensor to stepwise increase of the NO_2 concentration from 0 to 160ppb at optimum operating temperature is shown in Fig. 5a. The inset is the resistance transient in the presence of only 80ppb of NO_2 . It is obvious that the resistance increases when exposed to the gradually increased concentration of NO_2 . In other words, the response increases with the increasing of the concentration. The relationship between the response of the sensor and the concentration of NO_2 is shown in Fig. 5b, the error bars are also

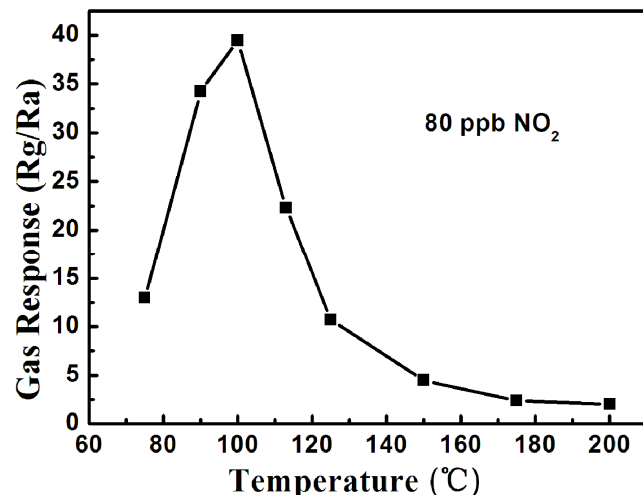


Fig. 4. Correlations between the gas response and response time to 80 ppb NO₂ and the operating temperature for the sensor using the as-obtained WO₃.

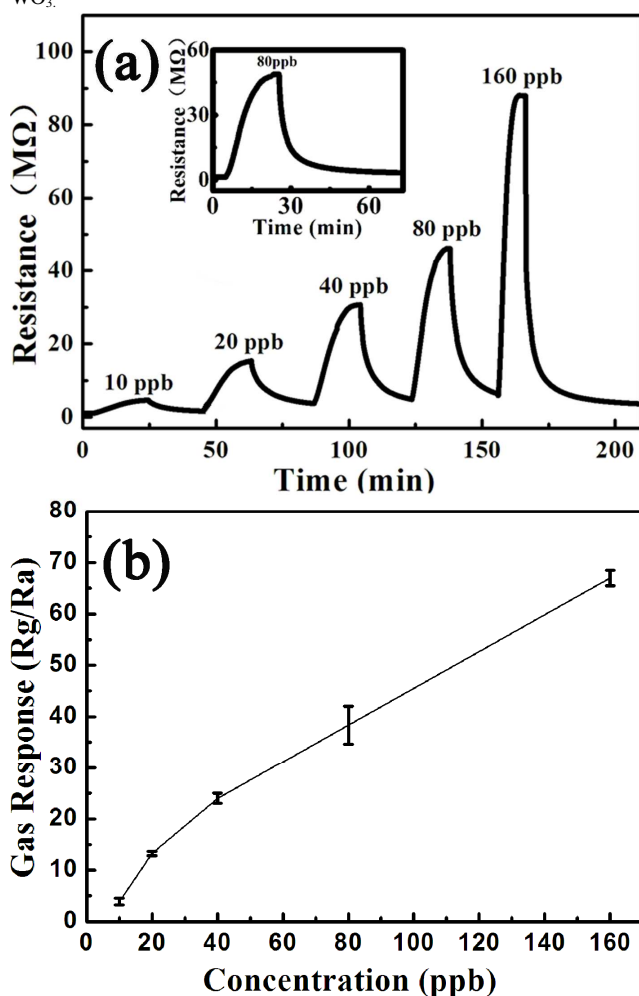


Fig. 5. (a) Response transients of the sensor to different NO₂ concentration at 100°C. (b) Gas response of the sensor as a function of NO₂ concentrations. Error bars are the standard deviations.

displayed. The error bars represent the standard deviation at a fixed concentration and they are small in all cases, which mean a low experimental variability. It is worth noting that this sensor

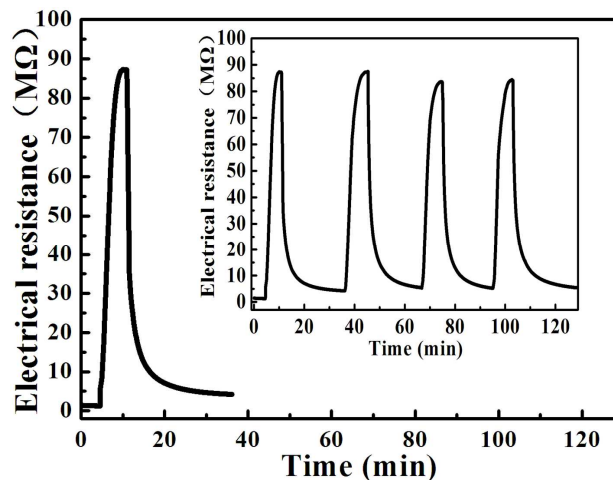


Fig. 6. Response transients of the sensor to 160 ppb NO₂ at 100°C, the inset displaying four periods of response curve.

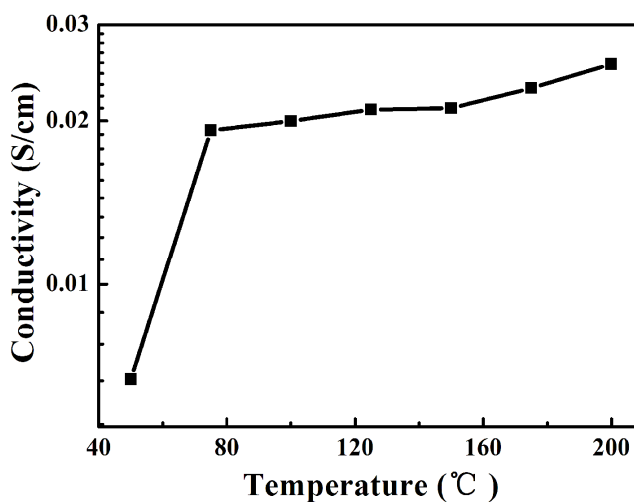


Fig. 7. Conductivity of the sensor as a function of operating temperature.

has response to low concentration of NO₂, and even the 10 ppb NO₂ can also be detected. The response transients of the sensor to 160 ppb NO₂ was measured at 100°C (Fig. 6). The four reversible cycles of the response curve indicates a stable and repeatable characteristic, as shown in the inset of Fig. 6. A comparison between the sensing performances of the sensor fabricated in our work and literature reports is summarized in Table 1. From comparison, it can be seen that the sensor based on cuboid WO₃ crystals has a correspondingly high response and low operating temperature. The high response of this cuboid nanobulks material may be attributed to the following reasons. On one hand, the product has a good crystalline character. The high crystallization will result in low bulk defects, which lead to the low conductivity of the sensing body. Due to this reason, only a small amount of NO₂ adsorption will cause the resistance changed greatly. The conductivity of the sensor with the variation of operating temperature is also shown in Fig. 7, it can be clearly observed that the conductivities change greatly between 50°C and 75°C, and then slowly increased between 75°C and 200°C. On the other hand, the cuboid structure has the trim edges, which will form the grain boundaries in the sensing body. According to Li et al.³³ and Hyodo et al.³⁴, grain boundaries or grain junctions are considered as the active sites and they act positively on the sensor response. Therefore, the sensor is expected to have high response to NO₂.

Table 1

Gas responses to NO₂ in the present study and those reported in the literatures

| Material | Preparation | NO ₂ concentration | Operating temperature | Response | Reference |
|-----------------|---------------------|-------------------------------|-----------------------|----------|---------------|
| WO ₃ | hydrothermal | 40 ppb | 100□ | 23 | Present study |
| WO ₃ | acidification | 50 ppb | 200□ | 13 | [29] |
| WO ₃ | Thermal evaporation | 100 ppb | 100□ | 18.2 | [30] |
| WO ₃ | Template method | 1 ppm | 230□ | 9 | [31] |
| WO ₃ | hydrothermal | 1 ppm | 200□ | 13.4 | [32] |

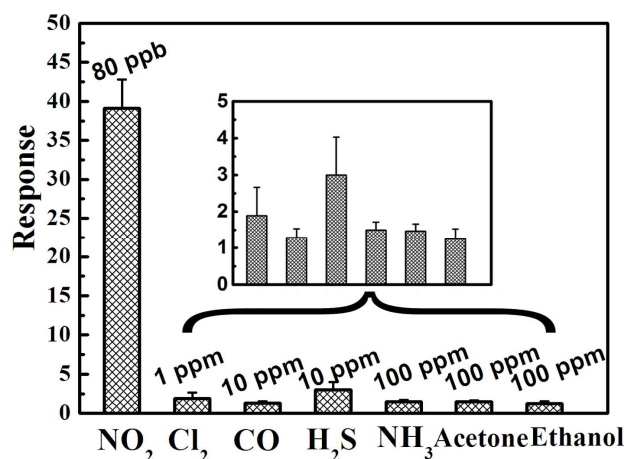


Fig. 6. Comparison of responses of the sensor based on WO₃ to various gases at 100°C. Error bars represent the variability obtained in measurements.

As is well known that the selectivity is another important parameter of a sensor in the view of practical application, therefore, at the optimum operating temperature, the response of the sensor based on the cuboid nanobulks to various kinds of gases was investigated, such as Cl₂, CO, H₂S, NH₃, acetone and ethanol. The results are shown in Fig. 7 with error bars. It can be seen that the sensor has a high response to NO₂ compared to the other gases. Such result demonstrates that the sensor using the WO₃ nanostructure synthesized here exhibits an excellent selectivity to NO₂ against the other tested gases at the working temperature of 100°C.

4. Conclusion

In summary, cuboid WO₃ crystal has been successfully synthesized through a simple one-step solution route combined with a subsequent calcining process. Field emission scanning electron microscopic and transmission electron microscopy results demonstrate that the products are composed of nanobulks and they are single crystal. In addition, the gas sensing properties of sensors based on calcined WO₃ toward NO₂ were investigated. The sensor based on the cuboid WO₃ nanobulks exhibits excellent NO₂ sensing properties at 100°C. In particular, the response to 40 ppb could achieve 23 at 100□. These results indicate that our sensor might have potential application to fabricate highly sensitive and low power consumption NO₂ gas sensor devices.

This work is supported by Application and Basic Research of Jilin Province (20130102010JC), the National Nature Science Foundation of China (No. 61304242, 61327804, 61134010 and 61374218), Program for Chang Jiang Scholars

and Innovative Research Team in University (No. IRT13018) and “863” High Technology Project (2013AA030902).

Notes and references

a State Key Laboratory on Integrated Optoelectronics, College of Electronic Science and Engineering, Jilin University, Changchun 130012, People's Republic of China. Fax: +86 431 85167808; Tel: +86 431 85167808; E-mail: syf@jlu.edu.cn, luyg@jlu.edu.cn

b State Key Laboratory of Luminescence and Application, Changchun Institute of Optics, Fine Mechanics and Physics, Chinese Academy of Sciences, Changchun 130033, China

References:

- 1 N. Yamazoe, G. Sakai and K. Shimanoe, *Catal. Surv. Asi.*, 2003, 7, 63-75.
- 2 N. Yamazoe, *Sens. Actuators, B*, 1991, 5, 7-19.
- 3 S.E. Lewis, J.R. DeBoer, J.L. Gole, P.J. Hesketh, *Sens. Actuators, B*, 2005, 110, 54-65.
- 4 L. Boarino, C. Baratto, F. Geobaldo, G. Amato, E. Comini, A.M. Rossi, G. Faglia, G. Léronel, G. Sberveglieri, *Mater. Sci. Eng., B*, 2000, 69-70, 210-214.
- 5 Otto S, Wolfbeis, *Anal. Chem.*, 2006, 78, 3859-3874.
- 6 R.C. Jorgenson, S.S. Yee, *Sens. Actuators, B*, 1993, 12, 213-220.
- 7 L. Torsi, A. Dodabalapur, L. Sabbatini, P.G Zambonin, *Sens. Actuators, B*, 2000, 67, 312-316.
- 8 K.H. An, S.Y. Jeong, H.R. Hwang, Y.H. Lee, *Adv. Mater.*, 2004, 16, 1005-1009.
- 9 B. Bhoologa Rao, *Mater. Chem. Phys.*, 2000, 64, 62-65.
- 10 S. Roy, S. Basu, *Bull. Mater. Sci.*, 2002, 25, 513-515.
- 11 J. Watson, *Sens. Actuators, B*, 1984, 5, 29-42.
- 12 A. Maiti, J.A. Rodriguez, M. Law, P. Kung, J.R. McKinney, P.D. Yang, *Nano Lett.*, 2003, 3, 1025-1028.
- 13 J.T. Zhang, J.F. Liu, Q. Peng, X. Wang, Y.D Li, *Chem. Mater.*, 2006, 18, 867-871.
- 14 Y.S. Kim, I.S. Hwang, S.J. Kim, C.Y. Lee, J.H. Lee, *Sens. Actuators, B*, 2008, 135, 298-303.
- 15 J. Chen, L. Xu, W. Li, X. Gou, J. Chen, L. Xu, W. Li, X. Gou, *Adv. Mater.*, 2005, 17, 582-586.
- 16 P. Sun, Y.W. Liu, X.W. Li, Y.F. Sun, X.S. Liang, F.M. Liu, G.Y. Lu, *RSC Adv.*, 2012, 2, 9824-9829

- 17 T. Waitz, T. Wagner, T. Sauerwald, C.D. Kohl, M. Tiemann, *Adv. Funct. Mater.*, 2009, 19, 653-661.
- 18 X.M. Xu, X. Li, W.B. Wang, B. Wang, P. Sun, Y.F. Sun, G.Y. Lu, *RSC Adv.*, 2014, 4, 4831-4835.
- 19 X.L. Li, T.J. Lou, X.M. Sun and Y. Dong Li, *Inorg. Chem.*, 2004, 43, 5442-5449.
- 20 B.B. Cao, J.J. Chen, X.J. Tang, W.L. Zhou, *J. Mater. Chem.*, 2009, 19, 2323-2327.
- 21 J.M. Ma, J. Zhang, S.R. Wang, T.H. Wang, J.B. Lian, X.C. Duan, W.J. Zheng, *J. Phys. Chem. C*, 2011, 115, 18157-18163.
- 22 J.M. Wang, E. Khoo, P.S. Lee, J. Ma, *J. Phys. Chem. C*, 2008, 112, 14306-14312.
- 23 Q.J. Sun, J.M. Luo, Z.F. Xie, J.D. Wang, X.T. Su, *Mater. Lett.*, 2008, 62, 2992-2994.
- 24 J.R. Huang, X.J. Xu, C.P. Gu, G.J. Fu, W.Z. Wang, J.H. Liu, *Mater Res. Bull.*, 2012, 47, 3224-3232.
- 25 J. Zhou, Y. Ding, S.Z. Deng, L.G. Ning, S. Xu, Z.L. Wang, *Adv. Mater.*, 2005, 17, 2110-2114.
- 26 Y. Djaoued, S. Balaji, *J Sol-Gel Sci Technol*, 2013, 65, 374-383.
- 27 J. Zhang, J.P. Tu, X.H. Xia, X.L. Wang, C.D. Gu, *J. Mater. Chem.*, 2011, 21, 5492-5498.
- 28 A. Phuruangrat, D.J. Ham, S.J. Hong, S. Thongtem, J.S. Lee, *J. Mater. Chem.*, 2010, 20, 1683-1690.
- 29 T. Kida, A. Nishiyama, M. Yuasa, K. Shimanoe, N. Yamazoe, *Sens. Actuators, B*, 2009, 135, 568-574.
- 30 A. Ponzoni, E. Comini, M. Ferroni, G. Sberveglieri, *Thin Solid Films*, 2005, 490, 81-85.
- 31 E. Rossinyol, A. Prim, E. Pellicer, J. Arbiol, F.H. Ramírez, F. Peiró, A. Cornet, J.R. Morante, L.A. Solovyov, B. Tian, T. Bo, D.Y. Zhao, *Adv. Funct. Mater.*, 2007, 17, 1801-1806.
- 32 Y.X. Qin, M. Hu, J. Zhang, *Sens. Actuators, B*, 2010, 150, 339-345.
- 33 E. Li, Z.X. Cheng, J.Q. Xu, Q.Y. Pan, W.J. Yu, Y.L. Chu, *Cryst. Growth Des.*, 2009, 9, 2146-2151.
- 34 T. Hyodo, N. Nishida, Y. Shimizu, M. Egashira, *Sens. Actuators, B*, 2002, 83, 209-215.
- 35 G. Lu, N. Miura, N. Yamazoe, *Ionics*, 1998, 4, 16-24.
- 36 X.Q. An, J.C. Yu, Y. Wang, Y.M. Hu, X.L. Yu, G.J. Zhang, *J. Mater. Chem.*, 2012, 22, 8525-8531.
- 37 A.P. Lee, B.J. Reedy, *Sens. Actuators, B*, 1999, 60, 35-42.